

Towards Continual, Online, Unsupervised Depth

Muhammad Umar Karim Khan
 Dexelon
 Daejeon, South Korea
 umar@kaist.ac.kr

Abstract

Although depth extraction with passive sensors has seen remarkable improvement with deep learning, these approaches may fail to obtain correct depth if they are exposed to environments not observed during training. Online adaptation, where the neural network trains while deployed, with unsupervised learning provides a convenient solution. However, online adaptation causes a neural network to forget the past. Thus, past training is wasted and the network is not able to provide good results if it observes past scenes. This work deals with practical online-adaptation where the input is online and temporally-correlated, and training is completely unsupervised. Regularization and replay-based methods without task boundaries are proposed to avoid catastrophic forgetting while adapting to online data. Experiments are performed on different datasets with both structure-from-motion and stereo. Results of forgetting as well as adaptation are provided, which are superior to recent methods. The proposed approach is more inline with the artificial general intelligence paradigm as the neural network learns the scene where it is deployed without any supervision (target labels and tasks) and without forgetting about the past. Code is available at github.com/umarKarim/cou_stereo and github.com/umarKarim/cou_sfm.

1. Introduction

Promisingly, deep learning mimics the human behavior from certain perspectives, though much is yet to be achieved. It has been instrumental in a wide variety of applications. Moreover, the results of deep learning reflect our behavior much better compared to classic algorithms. Catastrophic forgetting [29] and online adaptation are two specific examples of this. Neural networks are much better at recalling recent information compared to the distant past. Similarly, neural networks require special mechanisms to retain past information.

Extracting depth of a scene is critical for scene percep-

tion. Depth serves a wide variety of applications from computational photography to navigation. Active sensors such as LIDAR or time-of-flight are capable of providing results at depth resolutions better than the human vision system. However, these have numerous challenges such as low spatial resolution, interference, and high power consumption. Efforts have been made towards passive sensors replicating the human vision system. For example, stereo cameras, structure-from-motion (SfM) and monocular methods replicate binocular vision, head motion and object-size information for depth extraction, respectively.

Despite the widely-acclaimed success of deep learning, generalization towards unseen samples has proven to be a major problem. This problem is usually tackled by training over a dataset that covers as much of the possible samples as possible. For example, MiDaS [39] adopts this strategy and produces great results for a wide variety of scenes. However, there is still a possibility of an edge case that can prove to be catastrophic. Furthermore, any small addition to the training data requires performing retraining over the whole dataset again.

A different approach towards generalization is to allow the neural network to be always in an active, learning state. In other words, the neural network learns about the scene where it is deployed while not forgetting past information. This approach not only allows generalization to new domains but also does not require retraining. Thus, edge devices can autonomously learn without being connected to a centralized system.

The above paradigm shift comes with numerous challenges. Directly learning new tasks causes catastrophic forgetting of past tasks. Thus, the performance may improve on the new domain but the system will have relearn once it is used in the past domain. Also, in conventional training, samples are passed as a batch and repeatedly used with shuffling to train the neural network. However, in the above setting, only one sample is available at a time and that cannot be used repeatedly to train the neural network. Furthermore, task boundaries are not available, i.e., there is no supervision about when a new scene starts. Finally, it is

not practical to provide labels for training for every or any sample.

Numerous notable approaches have been proposed for the above challenges separately. These include continual, online, task-free continual, and unsupervised learning. However, little effort has been made towards solutions that can tackle all these problems together. Furthermore, evaluations have been limited to small and simple datasets in general.

This paper aims towards providing a unified solution to the above challenges for depth extraction. Our key contributions are as follows.

- A novel regularization and replay-based method for online learning of depth while avoiding catastrophic forgetting is proposed.
- Numerous practical constraints such as unsupervised learning, no task (scene) labels, no test-time oracle (where task information is available at test time), temporally-correlated input, synchronous operation and fixed memory are applied.
- Experiments are conducted on both SfM and stereo, which show the plasticity (online adaptation) and stability (forgetting) performance under the same settings for challenging datasets.

Although this work is limited to depth extraction, the principles proposed here can be used in any downstream unsupervised task. Successful implementation of the proposed method on edge devices provides a step closer to artificial general intelligence, where devices can learn and make decisions on their own while deployed.

2. Related Work

2.1. Depth Estimation

Self-supervised training for stereo-based depth estimation is based on reconstructing one stereo image (or depth map) from the other [16, 17]. Similar approaches have been proposed for monocular or SfM approaches [55, 18], where the next or previous frame is reconstructed using depth and pose estimated by neural networks. [19] proposes excluding the occluded regions in training for SOTA results. Wasserstein distance is used in [15] for depth estimation and 3D object detection. Authors in [24] propose a self-supervised scheme to estimate the depth and 3D scene flow simultaneously. Multi-camera systems have been proposed in [51, 25] to increase depth range. [38] proposes a method to measure confidence of self-supervised depth estimation. In [49], authors use classical stereo approaches to improve performance of monocular depth estimation schemes. In [43], authors propose features for self-supervised depth estimation that are robust to the changes in domain. SLAM

and monocular depth estimation are used together to improve each other in [44]. In [5], stereo depth is estimated by binary classification. Removing camera rotations [54] and textured patches [50] have been used for depth estimation of indoor scenes.

2.2. Continual and Online Learning

In continual learning, a neural network learns new tasks while not forgetting about the old ones. Broadly, these methods use distillation [32, 14], regularization [29, 2], replay [41, 21] or their combination [35]. Regularization-based methods penalize changes to important weights or add new computational nodes to the neural network with a new task. Replay-based schemes feed past data to neural networks while learning the new task. The effect of different training regimes on catastrophic forgetting has been analyzed in [34]. [8] proposes a continual learning method with constant memory, no test-time oracle and without task boundaries. In [10], fast adaptation and recall are achieved for continual learning. [11] proposes to determine the instance of an input sample and use it to train the network accordingly. Knowledge transfer in similar tasks is dealt with in [27]. [23] deals with continual learning where new tasks may contain samples from old tasks. [1] gates layers based on the current task and also predicts tasks at inference. [48] proposes an online learning method for detecting interesting scenes for mobile robots. [12] proposes a method to perform continual learning with temporally-correlated data streams and [3] uses the loss curve to define task boundaries. [22] and [36] use network features to partially update the neural network for fast operation.

2.3. Continual and Online Learning of Depth

Numerous authors have worked towards the domain adaptation problem for depth estimation. In [51] and [53], authors propose a method to adapt from synthetic datasets to real datasets. In [45], the authors propose using conventional stereo matching algorithms for domain adaptation. To speed up the process, authors propose modular adaptation in [47]. Authors in [46] propose a meta-learning objective to quickly adapt to new scenes. Their work has been advanced in [52], where the authors develop an approach to perform online adaptation without catastrophic forgetting. [30] uses replay at test time. Note that [46], [52] and [30] perform adaptation on test data. Furthermore, [47] resets the neural network for every test sequence.

2.4. This Work

Methods have been proposed that deal with the challenges listed in Fig. 1, however, it is rare to find methods which deal with all these challenges together, thereby, limiting their utility. Methods that continually learn depth either present results of forgetting or adaptation for sepa-

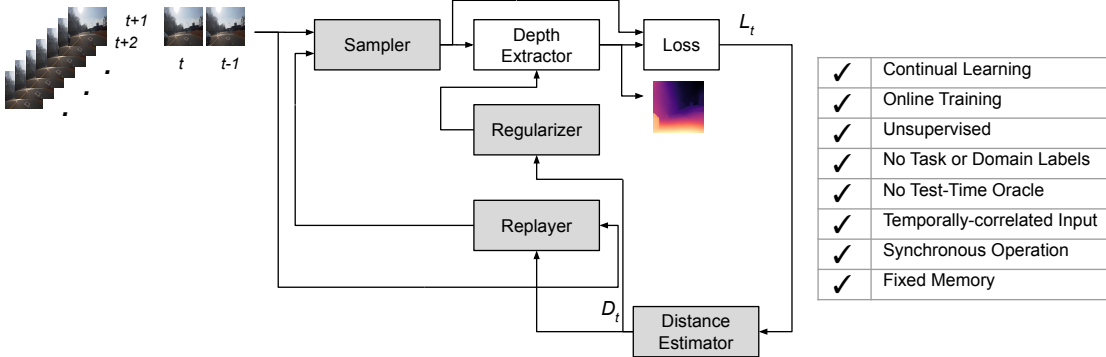


Figure 1. A graphical description of the proposed method. The non-shaded blocks are from conventional unsupervised depth-extraction schemes. The shaded blocks allow continual and online operation.

rate experiments. Thus, it is not possible to analyze the plasticity-stability compromise. Generally, similar datasets are used to evaluate online adaptation from one dataset to another and test data adaptation is performed. In this work, both adaptation and forgetting are analyzed over different datasets without adaptation over the test data.

3. Soft Task-Boundaries

Unlike general continual learning research, the task boundaries are unknown which is more practical. Task in current setting can be considered as a domain. For example, day time images represent a different task compared to night images. Similarly, indoor scenes represent a different task compared to outdoor scenes.

The profile of the loss can provide us with valuable hints towards task boundaries. A converged loss is expected to remain stable over a period of time. A significant change in the loss value may indicate that the task has changed.

Let $L^{(t)}$ be a random variable indicating the loss value at time t . It is assumed

$$L^{(t)} \sim \mathcal{N}(\mu_t, \sigma_t), \quad (1)$$

with μ_t and σ_t the corresponding mean and standard deviation, respectively. The log-probability that sample t belongs to a different task compared to $t-1$ is given by

$$\log P(T(t) \neq T(t-1)) = \frac{1}{2} D_t(L^{(t-1)}, L_t(x_t; \theta_t)) + c, \quad (2)$$

where $T(t)$ is the task at time t , $c = \log(\sigma_{t-1} \sqrt{2\pi})$, θ_t represent the network parameters and D_t is the squared Mahalanobis distance given by

$$D_t(L^{(t-1)}, L_t(x_t; \theta_t)) = \frac{(L_t(x_t; \theta_t) - \mu_{t-1})^2}{\sigma_{t-1}^2}. \quad (3)$$

In detail, the log-probability of a new task at time t depends on how far the current observed loss L_t is from the loss distribution of $L^{(t-1)}$. The parameters are updated iteratively using a low-pass filter as

$$\mu_t = \mu_{t-1} + \alpha_L (L_t - \mu_{t-1}) \quad (4)$$

and

$$\sigma_t^2 = \sigma_{t-1}^2 + \alpha_L (L_t - \mu_{t-1})^2, \quad (5)$$

where α_L is a constant. The loss profile has been used to define task boundaries in the past as well [3]. However, current approach is significantly different from [3] in that they use plateaus and peaks of the loss profile to determine a task boundary whereas here just the Mahalanobis distance is used. Furthermore, they use hard task-boundaries whereas proposed algorithms can use the Mahalanobis distance as a representation of the probability of the task boundary. In other words, soft task-boundaries are used here.

4. Regularization with Soft Task-Boundaries

Regularization for continual learning limits changes to the network architecture or parameters across tasks to retain information about previous tasks. Memory-aware synapses (MAS) [2] is a common approach towards regularization for continual learning across tasks. MAS assigns importance to parameters based on how changing them changes the output for a given input. At the beginning of every new task, they pass an input sample through the neural network and assign importance to each parameter based on the gradient of the parameters. This creates numerous problems for practical applications. First, hard task-boundaries are required. Second, an additional forward-backward pass is performed at the end of each task. Last, training is not synchronized with the input data due to additional delay at the end of each task.

In this work, a different definition of importance is used. In neural network compression techniques such as pruning,

parameter values close to zero are compressed while larger parameter values are not [31]. This is quite intuitive as a parameter with larger magnitude will affect the output more than a parameters with smaller magnitude. Thus, the importance of the i -th parameter is given by

$$\Omega_{i,t} = \|\theta_{i,t-1}\|, \quad (6)$$

where θ_i is the i -th parameter of the network. The regularization loss is computed as

$$L_t^{(reg)}(\theta) = \sum_i \Omega_{i,t} \|\theta_i - \theta_{i,t-1}\|, \quad (7)$$

and the combined loss is given by

$$L_t^{(tot)}(x_t, \theta) = L_t(x_t; \theta) + \gamma D_t L_t^{(reg)}(\theta), \quad (8)$$

where γ is a constant. In detail, the penalty imposed on the weights depends on both the importance of the weights as well as the chance of a new task at time t . In other words, the method is more conservative about changing the important parameters if the chances of a new task are higher. This approach assists in both remembering past tasks as well as forward transfer. Also, this approach does not require hard task boundaries and additional forward-backward passes. Note that θ with subscript t represents the current constant value of the parameters whereas θ without the subscript t represents the decision variable.

5. Replay with Soft Task-Boundaries

Let T represent the current task. A general representation of the loss function for the task T with regularization is given by

$$L_T^{(ov)} = L_T^{(curr)} + \gamma L_T^{(prev)}. \quad (9)$$

Minimizing $L_T^{(curr)}$ and $L_T^{(prev)}$ is equivalent to improving performance on the current and previous tasks, respectively. The loss on the previous task can be similarly given as

$$L_T^{(prev)} \equiv L_{T-1}^{(ov)} = L_{T-1}^{(curr)} + \gamma L_{T-1}^{(prev)}. \quad (10)$$

Thus, the contribution of the n -th previous task to the current loss function is $n\gamma$. Generally, γ is set to less than one, therefore, in theory it is expected that the performance over distant tasks will decrease more compared to recent tasks if regularization is used only.

To assign equal importance to all past tasks, replay is used. The choice of samples to be used for replay is based on the Mahalanobis distance. Samples are stored in the replay memory if D_t is greater than one. By using this approach, difficult examples are saved from which the network can learn more [12]. Based on [22], the storage capacity is limited to 1.5GB. If at full capacity, the new sample

replaces a randomly-chosen old sample. Experiments show that the replay buffer consumes much less storage than the upper limit.

The choice of storing original images to memory is based on numerous factors. Generally, replay is performed by using a generative network [41]. For classification problems, generative replay may work well as classification is based on more abstract features. Depth extraction, on the other hand, is based on pixel-level disparities which are difficult to recreate. Furthermore, generative replay requires significant amount of additional computational power which may not be practical. Some authors [22] propose storing compressed intermediate features of the neural network and their corresponding target labels for partially updating the neural network. However, storing target labels is not possible in the current case due to two reasons. Such an approach will require storing the corresponding compressed representation for the output depth map. Second, their are no guarantees that the stored depth maps are accurate enough to be used as targets. Therefore, actual inputs are stored for replay.

The replay and online samples are input to the neural network with the same probability. By this the paradigm of spaced repetition [4] is followed where difficult examples are taught to a learning system spaced over time.

6. Replay vs Regularization

Both regularization and replay have their pros and cons. Regularization requires additional memory and computations to maintain the importance of the parameters. Replay does not require significant amount of computational power, however, it needs space to store past samples. Therefore, replay can be used when sufficient storage is available and read/write is fast. Note that both the proposed regularization and replay are used together in this work.

7. Unsupervised Depth Extraction

The proposed approaches are applied to both unsupervised stereo and SfM-based depth extraction schemes. In the following, the subscript t is skipped for brevity.

7.1. Unsupervised Stereo

Depth extraction with stereo cameras is based on disparity estimation across rectified left and right images. The relationship between left and right images is given by

$$I_l(x + d(x, y), y) = I_r(x, y), \quad (11)$$

where I_l , I_r , and d denote the left image, right image, and disparity map, respectively. A neural network is trained to implicitly learn the disparity by trying to reconstruct the right image. I.e.,

$$d = \mathcal{F}_d(I_l; \theta), \quad (12)$$

which can be used to reconstruct the corresponding right image as

$$I'_r = f_w(I_l; d), \quad (13)$$

where \mathcal{F}_d represents the disparity neural network and f_w represents the warping function followed by bilinear interpolation [26]. The reconstruction loss is then given by

$$L = L_p(I'_r, I_r) + \beta_{ss} L_{ss}(I'_r, I_r) + \beta_s L_s(d, I_l), \quad (14)$$

where L_p , L_{ss} , and L_s are pixel-wise, SSIM and smoothness losses, respectively. β_{ssim} and β_s are constants. Refer to [17, 18] for a discussion on these constants and losses. For the disparity generating neural network, a UNet-based [40] encoder-decoder architecture is used. The same disparity network as [6] is used. The approach is shown in Fig. 2.

Numerous techniques have been proposed which significantly improve the performance of unsupervised stereo. These include generating two disparity maps and reconstructing both images [17], and using cycle-GAN [37] among others. However, in this work the emphasis is on online operation, therefore, only the right image is reconstructed and GANs are not used.

7.2. Unsupervised Structure-from-Motion

For estimating depth using SfM, two separate networks are used. The first is used to generate the disparity map with a single frame as input. The second is used to generate the camera matrix with two frames as input, one as reference and the other as target. The target frame is reconstructed from the reference frame, disparity and camera matrix using the warping function [26]

$$I'_{tar} = f_w^{(c)}(I_{ref}; d, c), \quad (15)$$

where $f_w^{(c)}$ represents the warping function [26], d is the disparity, and c is the camera matrix. The approach is shown in Fig. 3. The current frame and previous frame are the target and reference, and vice versa. Eq. 14 is used to compute the loss between the reconstructed and original target frame. Geometric loss is used as in [6]. However, unlike [6] and majority of SfM-based deep learning approaches, the pose network learns both the camera intrinsics and extrinsics [20]. This allows for more flexible use as the intrinsics of the camera systems need not be calculated beforehand and the system can be used across cameras.

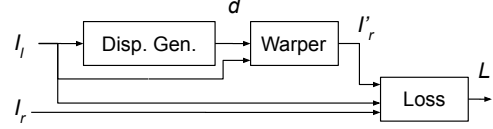


Figure 2. Block diagram of stereo-based disparity estimation where Disparity Generator is a neural network.

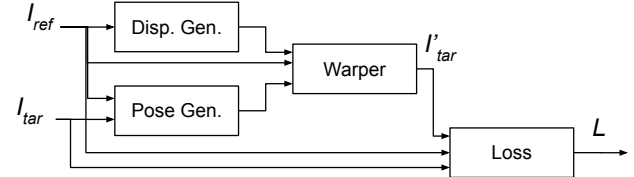


Figure 3. Block diagram of SfM-based disparity and pose estimation where Disparity Generator and Pose Generator are neural networks.

Pre-Train	Meth.	Onl. Train	Curr. Dist.	Cross Dist.	Online Adapt.	Cross Dom.
K+N	FT	K	0.1829	0.2852	0.1925	0.2128
K+N	Prop.	K	0.1487	0.1937	0.1442	0.1566
K+N	FT	N	0.2515	0.3262	0.2317	0.2722
K+N	Prop.	N	0.1922	0.1727	0.1738	0.1895

Table 1. Absolute Relative of SfM-based depth estimation. K , N and FT stand for KITTI, NYU and fine tuning, respectively.

Pre-Train	Meth.	Onl. Train	Curr. Dist.	Cross Dist.	Online Adapt.	Cross Dom.
K+vK	FT	K	0.3638	0.4606	0.2868	0.3223
K+vK	Prop.	K	0.2407	0.2375	0.2362	0.2225
K+vK	FT	vK	0.2526	0.2783	0.2406	0.2549
K+vK	Prop.	vK	0.2328	0.2365	0.2334	0.2375

Table 2. Absolute Relative of stereo-based depth estimation. K , vK and FT stand for KITTI, virtual KITTI and fine tuning, respectively.

8. Experimental Results

Since the proposed approach is for online learning and not based on the conventional approach of training followed by testing, therefore, some terminology and evaluation protocols are discussed first.

8.1. Datasets

For experiments, three datasets are used: KITTI [33], Virtual KITTI [9], and rectified New York University (NYU) v2 [42, 7] datasets. The Eigen test split [13] is used with KITTI. For the Virtual-KITTI dataset, the first 90% frames of every sequence are for training and the last 10% for evaluation. Refer to supplementary material for more details. These datasets are very different from each other,

and it is very difficult to generalize from one of these to another, therefore, these datasets provide better evaluation of the proposed approach.

8.2. Terminology

Each dataset is called a **distribution**. For example, NYU is from an indoor distribution, Virtual KITTI is from a synthetic distribution, and KITTI is from an outdoor distribution. Every scene in each dataset is treated as a separate **domain**. For example, road sequences in KITTI are from a different domain compared campus sequences. **Cross-distribution results** are obtained if online training and evaluation are performed on different datasets. **Cross-domain results** show the performance of previously seen domains of the current dataset during online training. **Online adaptation results** show the performance on the current domain over which training has been performed.

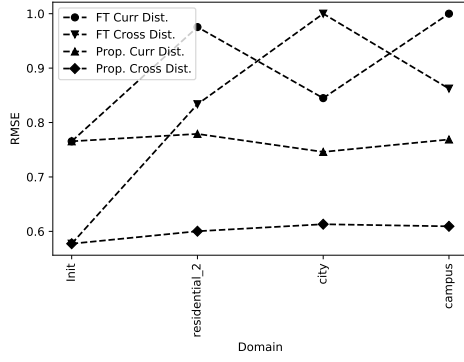


Figure 4. Evolution of performance with SfM-based online training on KITTI dataset. FT stands for fine tuning.

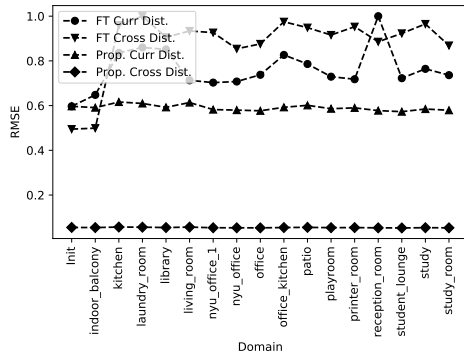


Figure 5. Evolution of performance with SfM-based online training on NYU dataset. FT stands for fine tuning.

8.3. Training and Evaluation Protocol

Training is divided into two stages: Pre-training and online training. Domains observed during pre-training are not

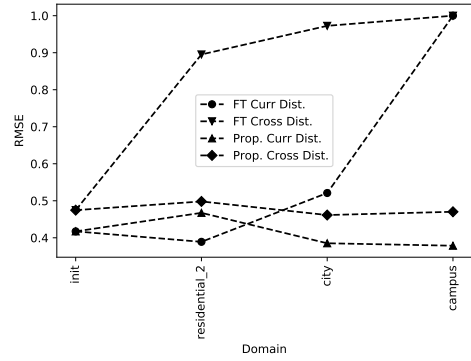


Figure 6. Evolution of performance with stereo-based online training on KITTI dataset. FT stands for fine tuning.

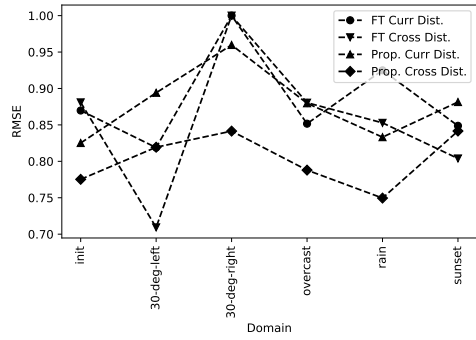


Figure 7. Evolution of performance with stereo-based online training on virtual KITTI dataset. FT stands for fine tuning.

observed during online training. Pre-training is the same as warming up [22] and is required for cross-distribution performance evaluation. It provides the base model for online training. For online training, data is sequentially passed and shuffling is not performed. Thus, temporal correlation is maintained which is more realistic but difficult to handle [12]. Proposed results are averaged over three runs of online training. The evaluation results are obtained by averaging the results of all frames of the test data. Refer to supplementary material for further details. The test data is not used for learning unlike [52, 46] but for evaluation only. In other words, there is no test-time oracle.

8.4. Setup

The same hyper-parameters and optimizer were used for all experiments. The Adam optimizer [28] is used with $\beta_1 = 0.9$, $\beta_2 = 0.99$, learning rate of 10^{-4} , batch size of 1, $\alpha_L = 0.1$, $\gamma = 10^{-2}$, $\beta_p = 0.15$, $\beta_{ss} = 0.85$, and $\beta_s = 0.1$. A single Nvidia GTX 1080Ti GPU was used for all the experiments. All frames are resized to 320×256 .

Meth.	Model	Test Adp.	RMSE \downarrow	Abs. Rel. \downarrow	δ (1.25) \uparrow	δ (1.25 2) \uparrow	RMSE \uparrow imp.
FT	[55]	Yes	6.5248	0.2070	0.7041	0.8806	0%
FT	[6]	Yes	5.6528	0.1735	0.7743	0.9140	0%
L2A [46]	[55]	Yes	6.3804	0.1937	0.7221	0.8980	2.21%
L2A [46]	[6]	Yes	5.5500	0.1692	0.7881	0.9197	1.82%
LPF [52]	[55]	Yes	6.1090	0.1794	0.7307	0.9126	6.37%
LPF [52]	[6]	Yes	5.4452	0.1505	0.7990	0.9325	3.67%
FT	Prop.	No	8.7184	0.3318	0.4853	0.7445	0%
Prop.	Prop.	No	<u>5.5483</u>	<u>0.1393</u>	<u>0.8213</u>	0.9413	36.36%
FT*	Prop.	No	7.7611	0.2498	0.6097	0.8371	0%
Prop.*	Prop.	No	5.6160	0.1376	0.8229	0.9403	27.63%

Table 3. Results of training with KITTI and then with virtual KITTI. *shows that `fog` and `rain` domains are included in online training. RMSE improvement shows the percent decrease in RMSE compared to fine tuning. Best result are bold and second best are underlined. Results of other methods are taken from [52].

8.5. Performance Evaluation

In the first set of experiments, pre-training is performed on roughly half of the KITTI and NYU datasets, and perform online training on either KITTI or NYU. The results are shown in Table 10. Online training on one dataset severely degrades performance on the other dataset if it is directly fine-tuned. However, by using the proposed approach of regularization and replay the neural network remembers information from the dataset it is not being trained on. Furthermore, online adaptation is not degraded, rather, the proposed method improves online adaptation. This should come as no surprise as regularization improves forward transfer of information and replay exposes the network to difficult examples, thus a better choice for plasticity and stability. The performance evolution over time for a single run of online training is shown in Fig. 4 and Fig. 5. Note that current and cross-distribution RMSE is normalized with maximum current and cross-distribution RMSE of fine-tuning, respectively in Fig. 4, 5, 6 and 7. The figures show that the performance remains consistent by using the proposed method compared to fine tuning. Qualitative results are shown in Fig. 8. Results with other metrics are in the supplement.

Please note that the the results shown here should not be compared with methods that follow the conventional paradigm of training followed by testing. With KITTI in conventional setting, the network is trained over the KITTI training data for multiple epochs and then evaluated over the test data. In the current scenario, the network is pre-trained over half of KITTI and NYU datasets for multiple epochs, and then trained over the other half of the KITTI dataset for one epoch only in online training.

For evaluation over stereo, pre-training is performed over half of the KITTI and virtual KITTI datasets, and online train on either KITTI or virtual KITTI datasets. The results are shown in Table 2 and evolution of performance

is shown in Fig. 6 and Fig. 7. Again we see significant improvement in performance with the proposed method. Qualitative results are shown in Fig. 9. Results with other metrics are in the supplementary material.

In [52], the authors perform experiments with SfM-based learning where they first pretrain the model with the KITTI dataset over multiple epochs and then online train over the virtual KITTI dataset for a single epoch. They also perform test-time adaptation, i.e., they use the sequences used for testing to learn while testing. Experiments with the proposed method are under a similar setting, however, test-time adaptation is not performed. Using the complete video sequence in testing provides useful context, which maybe taken test-time oracle. To avoid this discussion, adaptation on the test data is not done. Unlike [52], results with the `fog` and `rain` sequences of the virtual KITTI dataset are also included.

The experimental results are shown in Table 3. The proposed method outperforms competing methods except the RMSE metric despite using a smaller resolution for online operation and learning camera intrinsics. Note that the overall RMSE or results on other metrics are not representative of the plasticity-stability performance. For example, not learning anything about the virtual KITTI dataset while online training will provide best results on the KITTI dataset. This is clearly counter-intuitive. A better approach to measure performance is to see the percentage improvement compared to fine tuning. The percentage improvement by the proposed method is much superior compared to other methods.

The effect of regularization and replay is shown in Table 4. The table shows that the combination of replay and regularization provide the overall best results.

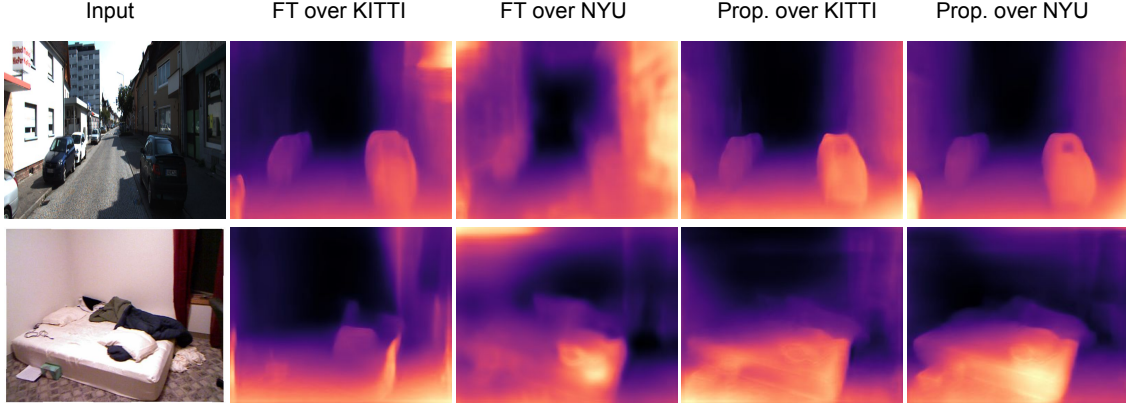


Figure 8. Qualitative results with SfM over KITTI and NYU datasets. Fine tuning over one dataset results in forgetting over the other dataset. However, the proposed method avoids catastrophic forgetting while improving performance. Best seen in color.

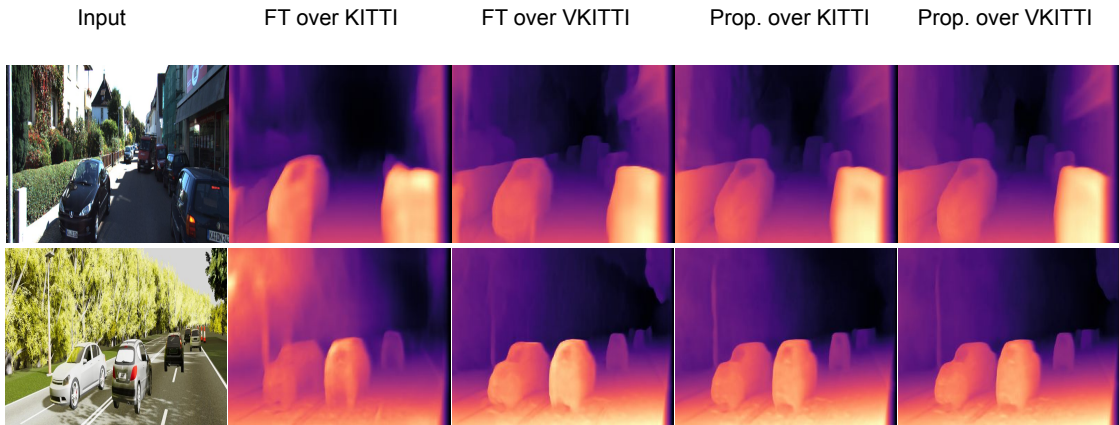


Figure 9. Qualitative results with stereo over KITTI and virtual KITTI datasets. Best seen in color.

Meth.	Data	Curr. Dist.	Cross Dist.	Online Adapt.	Cross Domain
FT	KITTI	7.4483	0.9734	6.2184	6.68
Reg.	KITTI	6.6603	0.6955	5.7572	5.7938
Rep.	KITTI	5.7583	0.6882	5.7482	5.735
Prop.	KITTI	5.7266	0.6878	5.3482	5.6507
FT	NYU	0.8103	10.3687	0.9473	1.0368
Reg.	NYU	0.8710	8.5240	0.9203	0.9343
Rep.	NYU	0.6368	7.3262	0.7582	0.7587
Prop.	NYU	0.6376	6.1025	0.7621	0.7572

Table 4. RMSE under with different components of the proposed approach for a single run. FT, Reg., Rep. and Prop. stand for fine tuning, regularization, replay and proposed method, respectively. KITTI + NYU was used for pre-training.

9. Conclusion

A method is presented for learning depth of a scene while deployed and not forgetting about the past. The approach is based on a combination of regularization and replay. The proposed method learns depth from a stream of video frames and avoids catastrophic forgetting. Experimental results show that the proposed method works with both structure-from-motion and stereo approaches. Quantitative results on multiple evaluation metrics are better compared to recent methods. The proposed method can be considered as a step towards autonomous scene-perception where the system learns about a scene without any supervision.

References

- [1] Davide Abati, Jakub Tomczak, Tijmen Blankevoort, Simone Calderara, Rita Cucchiara, and Babak Ehteshami Bejnordi. Conditional channel gated networks for task-aware continual learning. In *Proceedings of the IEEE/CVF Conference on Computer Vision and Pattern Recognition*, pages 3931–3940, 2020. [2](#)
- [2] Rahaf Aljundi, Francesca Babiloni, Mohamed Elhoseiny, Marcus Rohrbach, and Tinne Tuytelaars. Memory aware synapses: Learning what (not) to forget. In *Proceedings of the European Conference on Computer Vision (ECCV)*, pages 139–154, 2018. [2, 3](#)
- [3] Rahaf Aljundi, Klaas Kelchtermans, and Tinne Tuytelaars. Task-free continual learning. In *Proceedings of the IEEE/CVF Conference on Computer Vision and Pattern Recognition*, pages 11254–11263, 2019. [2, 3](#)
- [4] Hadi Amiri, Timothy Miller, and Guergana Savova. Repeat before forgetting: Spaced repetition for efficient and effective training of neural networks. In *Proceedings of the 2017 Conference on Empirical Methods in Natural Language Processing*, pages 2401–2410, 2017. [4](#)
- [5] Abhishek Badki, Alejandro Troccoli, Kihwan Kim, Jan Kautz, Pradeep Sen, and Orazio Gallo. Bi3d: Stereo depth estimation via binary classifications. In *Proceedings of the IEEE/CVF Conference on Computer Vision and Pattern Recognition*, pages 1600–1608, 2020. [2](#)
- [6] Jia-Wang Bian, Zhichao Li, Naiyan Wang, Huangying Zhan, Chunhua Shen, Ming-Ming Cheng, and Ian Reid. Unsupervised scale-consistent depth and ego-motion learning from monocular video. *arXiv preprint arXiv:1908.10553*, 2019. [5, 7](#)
- [7] Jia-Wang Bian, Huangying Zhan, Naiyan Wang, Tat-Jun Chin, Chunhua Shen, and Ian Reid. Unsupervised depth learning in challenging indoor video: Weak rectification to rescue. *arXiv preprint arXiv:2006.02708*, 2020. [5](#)
- [8] Pietro Buzzega, Matteo Boschini, Angelo Porrello, Davide Abati, and Simone Calderara. Dark experience for general continual learning: a strong, simple baseline. In *34th Conference on Neural Information Processing Systems (NeurIPS 2020)*, 2020. [2](#)
- [9] Yohann Cabon, Naila Murray, and Martin Humenberger. Virtual kitti 2, 2020. [5](#)
- [10] Massimo Caccia, Pau Rodriguez, Oleksiy Ostapenko, Fabrice Normandin, Min Lin, Lucas Page-Caccia, Issam Hadj Laradji, Irina Rish, Alexandre Lacoste, David Vázquez, et al. Online fast adaptation and knowledge accumulation (osaka): a new approach to continual learning. *Advances in Neural Information Processing Systems*, 33, 2020. [2](#)
- [11] Hung-Jen Chen, An-Chieh Cheng, Da-Cheng Juan, Wei Wei, and Min Sun. Mitigating forgetting in online continual learning via instance-aware parameterization. *Advances in Neural Information Processing Systems*, 33, 2020. [2](#)
- [12] Aristotelis Chrysakis and Marie-Francine Moens. Online continual learning from imbalanced data. In *International Conference on Machine Learning*, pages 1952–1961. PMLR, 2020. [2, 4, 6](#)
- [13] David Eigen, Christian Puhrsch, and Rob Fergus. Depth map prediction from a single image using a multi-scale deep network. *arXiv preprint arXiv:1406.2283*, 2014. [5](#)
- [14] Enrico Fini, Stéphane Lathuilière, Enver Sangineto, Moin Nabi, and Elisa Ricci. Online continual learning under extreme memory constraints. In *European Conference on Computer Vision*, pages 720–735. Springer, 2020. [2](#)
- [15] Divyansh Garg, Yan Wang, Bharath Hariharan, Mark Campbell, Kilian Q Weinberger, and Wei-Lun Chao. Wasserstein distances for stereo disparity estimation. 2020. [2](#)
- [16] Ravi Garg, Vijay Kumar Bg, Gustavo Carneiro, and Ian Reid. Unsupervised cnn for single view depth estimation: Geometry to the rescue. In *European conference on computer vision*, pages 740–756. Springer, 2016. [2](#)
- [17] Clément Godard, Oisin Mac Aodha, and Gabriel J Brostow. Unsupervised monocular depth estimation with left-right consistency. In *Proceedings of the IEEE Conference on Computer Vision and Pattern Recognition*, pages 270–279, 2017. [2, 5](#)
- [18] Clément Godard, Oisin Mac Aodha, Michael Firman, and Gabriel J Brostow. Digging into self-supervised monocular depth estimation. In *Proceedings of the IEEE/CVF International Conference on Computer Vision*, pages 3828–3838, 2019. [2, 5](#)
- [19] Juan Luis GonzalezBello and Munchurl Kim. Forget about the lidar: Self-supervised depth estimators with med probability volumes. *Advances in Neural Information Processing Systems*, 33, 2020. [2](#)
- [20] Ariel Gordon, Hanhan Li, Rico Jonschkowski, and Anelia Angelova. Depth from videos in the wild: Unsupervised monocular depth learning from unknown cameras. In *Proceedings of the IEEE/CVF International Conference on Computer Vision*, pages 8977–8986, 2019. [5](#)
- [21] Gunshi Gupta, Karmesh Yadav, and Liam Paull. La-maml: Look-ahead meta learning for continual learning. 2020. [2](#)
- [22] Tyler L Hayes, Kushal Kafle, Robik Shrestha, Manoj Acharya, and Christopher Kanan. Remind your neural network to prevent catastrophic forgetting. In *European Conference on Computer Vision*, pages 466–483. Springer, 2020. [2, 4, 6](#)
- [23] Jiangpeng He, Runyu Mao, Zeman Shao, and Fengqing Zhu. Incremental learning in online scenario. In *Proceedings of the IEEE/CVF Conference on Computer Vision and Pattern Recognition*, pages 13926–13935, 2020. [2](#)
- [24] Junhwa Hur and Stefan Roth. Self-supervised monocular scene flow estimation. In *Proceedings of the IEEE/CVF Conference on Computer Vision and Pattern Recognition*, pages 7396–7405, 2020. [2](#)
- [25] Saad Imran, Muhammad Umar Karim Khan, Sikander Bin Mukarram, and Chong-Min Kyung. Unsupervised monocular depth estimation with multi-baseline stereo. In *The 31st British Machine Vision Conference*. British Machine Vision Virtual Conference, 2020. [2](#)
- [26] Max Jaderberg, Karen Simonyan, Andrew Zisserman, and Koray Kavukcuoglu. Spatial transformer networks. *arXiv preprint arXiv:1506.02025*, 2015. [5](#)
- [27] Zixuan Ke, Bing Liu, and Xingchang Huang. Continual learning of a mixed sequence of similar and dissimilar tasks.

Advances in Neural Information Processing Systems, 33, 2020. 2

[28] Diederik P Kingma and Jimmy Ba. Adam: A method for stochastic optimization. *arXiv preprint arXiv:1412.6980*, 2014. 6

[29] James Kirkpatrick, Razvan Pascanu, Neil Rabinowitz, Joel Veness, Guillaume Desjardins, Andrei A Rusu, Kieran Milan, John Quan, Tiago Ramalho, Agnieszka Grabska-Barwinska, et al. Overcoming catastrophic forgetting in neural networks. *Proceedings of the national academy of sciences*, 114(13):3521–3526, 2017. 1, 2

[30] Yevhen Kuznetsov, Marc Proesmans, and Luc Van Gool. Comoda: Continuous monocular depth adaptation using past experiences. In *Proceedings of the IEEE/CVF Winter Conference on Applications of Computer Vision*, pages 2907–2917, 2021. 2

[31] Hao Li, Asim Kadav, Igor Durdanovic, Hanan Samet, and Hans Peter Graf. Pruning filters for efficient convnets. *arXiv preprint arXiv:1608.08710*, 2016. 4

[32] Zhizhong Li and Derek Hoiem. Learning without forgetting. *IEEE transactions on pattern analysis and machine intelligence*, 40(12):2935–2947, 2017. 2

[33] Moritz Menze and Andreas Geiger. Object scene flow for autonomous vehicles. In *Conference on Computer Vision and Pattern Recognition (CVPR)*, 2015. 5

[34] Seyed Iman Mirzadeh, Mehrdad Farajtabar, Razvan Pascanu, and Hassan Ghasemzadeh. Understanding the role of training regimes in continual learning. 2020. 2

[35] Pingbo Pan, Siddharth Swaroop, Alexander Immer, Runa Eschenhagen, Richard Turner, and Mohammad Emtiyaz Khan. Continual deep learning by functional regularisation of memorable past. 2020. 2

[36] Lorenzo Pellegrini, Gabriele Graffieti, Vincenzo Lomonaco, and Davide Maltoni. Latent replay for real-time continual learning. 2

[37] Andrea Pilzer, Dan Xu, Mihai Puscas, Elisa Ricci, and Nicu Sebe. Unsupervised adversarial depth estimation using cycled generative networks. In *2018 International Conference on 3D Vision (3DV)*, pages 587–595. IEEE, 2018. 5

[38] Matteo Poggi, Filippo Aleotti, Fabio Tosi, and Stefano Mattoccia. On the uncertainty of self-supervised monocular depth estimation. In *Proceedings of the IEEE/CVF Conference on Computer Vision and Pattern Recognition*, pages 3227–3237, 2020. 2

[39] René Ranftl, Katrin Lasinger, David Hafner, Konrad Schindler, and Vladlen Koltun. Towards robust monocular depth estimation: Mixing datasets for zero-shot cross-dataset transfer. *arXiv preprint arXiv:1907.01341*, 2019. 1

[40] Olaf Ronneberger, Philipp Fischer, and Thomas Brox. U-net: Convolutional networks for biomedical image segmentation. In *International Conference on Medical image computing and computer-assisted intervention*, pages 234–241. Springer, 2015. 5

[41] Hanul Shin, Jung Kwon Lee, Jaehong Kim, and Jiwon Kim. Continual learning with deep generative replay. In *Proceedings of the 31st International Conference on Neural Information Processing Systems*, pages 2994–3003, 2017. 2, 4

[42] Nathan Silberman, Derek Hoiem, Pushmeet Kohli, and Rob Fergus. Indoor segmentation and support inference from rgbd images. In *European conference on computer vision*, pages 746–760. Springer, 2012. 5

[43] Jaime Spencer, Richard Bowden, and Simon Hadfield. Defeat-net: General monocular depth via simultaneous unsupervised representation learning. In *Proceedings of the IEEE/CVF Conference on Computer Vision and Pattern Recognition*, pages 14402–14413, 2020. 2

[44] Lokender Tiwari, Pan Ji, Quoc-Huy Tran, Bingbing Zhuang, Saket Anand, and Manmohan Chandraker. Pseudo rgb-d for self-improving monocular slam and depth prediction. In *European Conference on Computer Vision*, pages 437–455. Springer, 2020. 2

[45] Alessio Tonioni, Matteo Poggi, Stefano Mattoccia, and Luigi Di Stefano. Unsupervised adaptation for deep stereo. In *Proceedings of the IEEE International Conference on Computer Vision*, pages 1605–1613, 2017. 2

[46] Alessio Tonioni, Oscar Rahnama, Thomas Joy, Luigi Di Stefano, Thalaiyasingam Ajanthan, and Philip HS Torr. Learning to adapt for stereo. In *Proceedings of the IEEE/CVF Conference on Computer Vision and Pattern Recognition*, pages 9661–9670, 2019. 2, 6, 7

[47] Alessio Tonioni, Fabio Tosi, Matteo Poggi, Stefano Mattoccia, and Luigi Di Stefano. Real-time self-adaptive deep stereo. In *Proceedings of the IEEE/CVF Conference on Computer Vision and Pattern Recognition*, pages 195–204, 2019. 2

[48] Chen Wang, Wenshan Wang, Yuheng Qiu, Yafei Hu, and Sebastian Scherer. Visual memorability for robotic interestingness via unsupervised online learning. In *European Conference on Computer Vision (ECCV)*. Springer, 2020. 2

[49] Jamie Watson, Michael Firman, Gabriel J Brostow, and Daniyar Turmukhambetov. Self-supervised monocular depth hints. In *Proceedings of the IEEE/CVF International Conference on Computer Vision*, pages 2162–2171, 2019. 2

[50] Zehao Yu, Lei Jin, and Shenghua Gao. P² net: Patch-match and plane-regularization for unsupervised indoor depth estimation. 2

[51] Kai Zhang, Jiaxin Xie, Noah Snavely, and Qifeng Chen. Depth sensing beyond lidar range. In *2020 IEEE/CVF Conference on Computer Vision and Pattern Recognition (CVPR)*, pages 1689–1697. IEEE, 2020. 2

[52] Zhenyu Zhang, Stéphane Lathuilière, Elisa Ricci, Nicu Sebe, Yan Yan, and Jian Yang. Online depth learning against forgetting in monocular videos. In *Proceedings of the IEEE/CVF Conference on Computer Vision and Pattern Recognition*, pages 4494–4503, 2020. 2, 6, 7

[53] Chuanxia Zheng, Tat-Jen Cham, and Jianfei Cai. T2net: Synthetic-to-realistic translation for solving single-image depth estimation tasks. In *Proceedings of the European Conference on Computer Vision (ECCV)*, pages 767–783, 2018. 2

[54] Junsheng Zhou, Yuwang Wang, Kaihua Qin, and Wenjun Zeng. Moving indoor: Unsupervised video depth learning in challenging environments. In *Proceedings of the IEEE/CVF International Conference on Computer Vision*, pages 8618–8627, 2019. 2

[55] Tinghui Zhou, Matthew Brown, Noah Snavely, and David G Lowe. Unsupervised learning of depth and ego-motion from video. In *Proceedings of the IEEE conference on computer vision and pattern recognition*, pages 1851–1858, 2017. [2](#), [7](#)

10. Datasets and Domains

Our aim is to divide the datasets into two parts: Pre-training and Online training. Domains are assigned to pre-training and online training such that the number of domains remains roughly the same in both.

10.1. SfM Experiments

10.1.1 KITTI Dataset

The KITTI dataset is already divided into multiple categories based on the location of the vehicle. Majority of these scenes are from the `residential` category. It is very difficult to have a reasonable division of the KITTI dataset based on categories. Thus, residential sequences were divided into two parts: `residential_1` and `residential_2`.

- Training frames: 44764
- Testing frames: 697
- Pre-training
 - Domains: Road, `residential_1`
 - Frames: 24920
- Online Training
 - Domains: `Residential_2`, city, campus
 - Frames: 19844

10.1.2 NYU Dataset

- Training frames: 69383
- Testing frames: 654
- Pre-training
 - Domains: From `basement` to `indoor_balcony`
 - Frames: 29596
- Online Training
 - Domains: The rest
 - Frames: 39787

10.2. Stereo Experiments

10.2.1 KITTI Dataset

- Training frames: 41888
- Testing frames: 697
- Pre-training
 - Domains: Road, `residential_1`

- Frames: 21696

- Online Training

- Domains: `Residential_2`, city, campus
 - Frames: 20192

10.2.2 vKITTI Dataset

- Training frames: 21620
- Testing frames: 2100
- Pre-training
 - Domains: 15-deg-left, 15-deg-right, clone, fog, morning
 - Frames: 9580
- Online Training
 - Domains: 30-deg-left, 30-deg-right, overcast, rain, sunset
 - Frames: 9580

10.3. Test Frames Categories

For vKITTI, the directory from which the frame is taken gives us the test frame category. The text file [here](#) was used for first finding the sequence to which the frame belongs, and then find the category to which the sequence belongs using the KITTI website. For NYU, the .mat file provided [here](#) was used to find the categories of the test frames.

11. Evaluation Metrics

Let N be the total number of pixels in a frame used for evaluation and x be the pixel index. Let d and d^* represent the obtained and the ground truth distance, respectively. Also, $1\{\cdot\}$ is the indicator function, which returns 1 if the condition in the parentheses is true, otherwise returns 0.

- **RMSE:** $\sqrt{\left(\frac{1}{N} \sum_x (d(x) - d^*(x))^2\right)}$
- **Absolute Relative:** $\frac{1}{N} \sum_x \frac{|d(x) - d^*(x)|}{d^*(x)}$
- **Square Relative:** $\frac{1}{N} \sum_x \frac{(d(x) - d^*(x))^2}{d^*(x)}$
- **Log RMSE:** $\frac{1}{N} \sum_x (\log(d(x)) - \log(d^*(x)))$
- $\delta(a): \frac{1}{N} \sum_x 1 \left\{ \max \left(\frac{d^*(x)}{d(x)}, \frac{d(x)}{d^*(x)} \right) < a \right\}$

12. Evaluation Protocol

The results in the manuscript are given for the whole dataset as well as domains within the dataset. These are described as follows.

12.1. Current Distribution Results

The results on the test data of the dataset over which training is performed. For example, if training is performed on KITTI then current distribution results show the results over the test data of KITTI dataset after online training is complete.

12.2. Cross-Distribution Results

The results on the test data of the dataset other than the one over which training is performed. For example, if training is performed on KITTI then cross distribution results show the results over the test data of NYU dataset after online training is complete.

12.3. Domain Results

Suppose the T -th domain is represented by D_T and the subset of test data frames from D_T is given by $F(D_T)$. Evaluation results on $F(D_T)$ are named as domain results of D_T .

12.4. Online Adaptation Results

Domain results of the most recent domain over which training has been performed are called online adaptation results.

12.5. Cross-Domain Results

Average of the domain results over the domains seen previously during training is called cross-domain result. Cross-domain results are given mathematically as

$$C_T = \frac{1}{T} \sum_t D_t \quad \forall t < T. \quad (16)$$

Note that previous domains also include domains of the current dataset used in pre-training.

13. Storage Requirements

It is noted that 320×256 .jpg images are approximately 20KB in size. This is the resolution used in our experiments. The number of frames stored for replay did not exceed 1500 in any of our experiments.

- KITTI + NYU SfM Experiments: The storage space required to maintain the pre-training dataset is approximately 1.04GB. An additional 12086 frames can be maintained for replay.
- KITTI + vKITTI SfM Experiments: The storage space required to maintain the pre-training dataset (KITTI) is approximately 0.85GB. An additional 16939 frames can be maintained for replay.

- KITTI + vKITTI Stereo Experiments: The storage space required to maintain the stereo pre-training dataset is approximately 1.19GB. An additional 8045 stereo images can be maintained for replay.

14. Additional Results

Pre-train	Method	Online Data	Curr. Dist.	Cross Dist.	Online Adapt.	Cross Domain
KITTI + NYU	Fine tune	KITTI	7.6117	0.9232	6.6861	6.6623
KITTI + NYU	Proposed	KITTI	5.6961 \pm 0.0951	0.6618 \pm 0.0104	5.6961 \pm 0.2234	5.7237 \pm 0.1731
KITTI + NYU	Fine tune	NYU	0.7925	10.2186	0.8810	1.0028
KITTI + NYU	Proposed	NYU	0.6349 \pm 0.0087	6.2240 \pm 0.2406	0.7381 \pm 0.0133	0.7501 \pm 0.0088

Table 5. RMSE of SfM-based depth estimation.

Pre-train	Method	Online Data	Curr. Dist.	Cross Dist.	Online Adapt.	Cross Domain
KITTI + NYU	Fine tune	KITTI	0.1829	0.2852	0.1925	0.2128
KITTI + NYU	Proposed	KITTI	0.1487 \pm 0.0026	0.1937 \pm 0.0041	0.1442 \pm 0.0034	0.1566 \pm 0.0029
KITTI + NYU	Fine tune	NYU	0.2515	0.3262	0.2317	0.2722
KITTI + NYU	Proposed	NYU	0.1922 \pm 0.0022	0.1727 \pm 0.0071	0.1738 \pm 0.0035	0.1895 \pm 0.0029

Table 6. Absolute Relative of SfM-based depth estimation.

Pre-train	Method	Online Data	Curr. Dist.	Cross Dist.	Online Adapt.	Cross Domain
KITTI + NYU	Fine tune	KITTI	1.5845	0.3379	1.4547	1.5466
KITTI + NYU	Proposed	KITTI	1.0792 \pm 0.0358	0.1747 \pm 0.0068	1.0277 \pm 0.0376	1.1149 \pm 0.0390
KITTI + NYU	Fine tune	NYU	0.2581	3.1456	0.2635	0.3453
KITTI + NYU	Proposed	NYU	0.1687 \pm 0.0029	1.3309 \pm 0.0118	0.1637 \pm 0.0082	0.1827 \pm 0.0049

Table 7. Square Relative of SfM-based depth estimation.

Pre-train	Method	Online Data	Curr. Dist.	Cross Dist.	Online Adapt.	Cross Domain
KITTI + NYU	Fine tune	KITTI	0.2899	0.3362	0.2754	0.2866
KITTI + NYU	Proposed	KITTI	0.2284 \pm 0.0011	0.2390 \pm 0.0030	0.2261 \pm 0.0066	0.2344 \pm 0.0054
KITTI + NYU	Fine tune	NYU	0.2956	0.4488	0.2714	0.3248
KITTI + NYU	Proposed	NYU	0.2346 \pm 0.0029	0.2532 \pm 0.0096	0.2151 \pm 0.0036	0.2384 \pm 0.0024

Table 8. Log RMSE of SfM-based depth estimation.

Pre-train	Method	Online Data	Curr. Dist.	Cross Dist.	Online Adapt.	Cross Domain
KITTI + NYU	Fine tune	KITTI	0.7129	0.5011	0.7161	0.6637
KITTI + NYU	Proposed	KITTI	0.7981 \pm 0.0026	0.7053 \pm 0.0059	0.8025 \pm 0.0101	0.7775 \pm 0.0090
KITTI + NYU	Fine tune	NYU	0.5946	0.4131	0.6358	0.5604
KITTI + NYU	Proposed	NYU	0.7225 \pm 0.0108	0.7437 \pm 0.0214	0.7328 \pm 0.0050	0.7054 \pm 0.0034

Table 9. $\delta(1.25)$ of SfM-based depth estimation.

Pre-train	Method	Online Data	Curr. Dist.	Cross Dist.	Online Adapt.	Cross Domain
KITTI + NYU	Fine tune	KITTI	0.8801	0.8096	0.8935	0.8824
KITTI + NYU	Proposed	KITTI	0.9322 \pm 0.0011	0.9141 \pm 0.0036	0.9312 \pm 0.0041	0.9290 \pm 0.0029
KITTI + NYU	Fine tune	NYU	0.8599	0.7203	0.8882	0.8312
KITTI + NYU	Proposed	NYU	0.9160 \pm 0.0031	0.9139 \pm 0.0066	0.9412 \pm 0.0047	0.9133 \pm 0.0028

Table 10. $\delta(1.25^2)$ of SfM-based depth estimation.

Pre-train	Method	Online Data	Curr. Dist.	Cross Dist.	Online Adapt.	Cross Domain
KITTI + vKITTI	Fine tune	KITTI	28.6678	12.6054	8.7470	9.7949
KITTI + vKITTI	Proposed	KITTI	7.5049 \pm 0.4482	6.7687 \pm 0.3425	5.5611 \pm 0.3946	5.4803 \pm 0.1539
KITTI + vKITTI	Fine tune	vKITTI	6.6617	6.7421	6.3894	6.6938
KITTI + vKITTI	Proposed	vKITTI	6.2629 \pm 0.0574	6.1279 \pm 0.2504	6.2727 \pm 0.2268	6.3615 \pm 0.2786

Table 11. RMSE of stereo-based depth estimation.

Pre-train	Method	Online Data	Curr. Dist.	Cross Dist.	Online Adapt.	Cross Domain
KITTI + vKITTI	Fine tune	KITTI	0.2842	0.2785	0.2116	0.2456
KITTI + vKITTI	Proposed	KITTI	0.1543 \pm 0.0009	0.1306 \pm 0.0003	0.1516 \pm 0.0073	0.1420 \pm 0.0077
KITTI + vKITTI	Fine tune	vKITTI	0.1388	0.1873	0.1312	0.1452
KITTI + vKITTI	Proposed	vKITTI	0.1250 \pm 0.0007	0.1481 \pm 0.0033	0.1267 \pm 0.0019	0.1305 \pm 0.0017

Table 12. Absolute Relative of stereo-based depth estimation.

Pre-train	Method	Online Data	Curr. Dist.	Cross Dist.	Online Adapt.	Cross Domain
KITTI + vKITTI	Fine tune	KITTI	35.1001	4.0265	3.5593	4.2980
KITTI + vKITTI	Proposed	KITTI	2.3681 \pm 0.4121	1.7574 \pm 0.2450	1.2135 \pm 0.1344	1.5055 \pm 0.1323
KITTI + vKITTI	Fine tune	vKITTI	1.6024	2.0815	1.6869	1.5398
KITTI + vKITTI	Proposed	vKITTI	1.4130 \pm 0.1195	1.7950 \pm 0.3160	1.4065 \pm 0.1554	1.4223 \pm 0.1398

Table 13. Square Relative of stereo-based depth estimation.

Pre-train	Method	Online Data	Curr. Dist.	Cross Dist.	Online Adapt.	Cross Domain
KITTI + vKITTI	Fine tune	KITTI	0.3638	0.4606	0.2868	0.3223
KITTI + vKITTI	Proposed	KITTI	0.2407 \pm 0.0016	0.2375 \pm 0.0024	0.2362 \pm 0.0048	0.2225 \pm 0.0055
KITTI + vKITTI	Fine tune	vKITTI	0.2526	0.2783	0.2406	0.2549
KITTI + vKITTI	Proposed	vKITTI	0.2328 \pm 0.0021	0.2365 \pm 0.0023	0.2334 \pm 0.0017	0.2375 \pm 0.0002

Table 14. Log RMSE of stereo-based depth estimation.

Pre-train	Method	Online Data	Curr. Dist.	Cross Dist.	Online Adapt.	Cross Domain
KITTI + vKITTI	Fine tune	KITTI	0.6799	0.5353	0.7222	0.6704
KITTI + vKITTI	Proposed	KITTI	0.8194 \pm 0.0039	0.8521 \pm 0.0050	0.8075 \pm 0.0143	0.8253 \pm 0.0137
KITTI + vKITTI	Fine tune	vKITTI	0.8532	0.7645	0.8529	0.8218
KITTI + vKITTI	Proposed	vKITTI	0.8580 \pm 0.0018	0.8197 \pm 0.0050	0.8567 \pm 0.0026	0.8479 \pm 0.0007

Table 15. $\delta(1.25)$ of stereo-based depth estimation.

Pre-train	Method	Online Data	Curr. Dist.	Cross Dist.	Online Adapt.	Cross Domain
KITTI + vKITTI	Fine tune	KITTI	0.8561	0.7723	0.8918	0.8612
KITTI + vKITTI	Proposed	KITTI	0.9309 \pm 0.0009	0.9405 \pm 0.0004	0.9304 \pm 0.0028	0.9394 \pm 0.0025
KITTI + vKITTI	Fine tune	vKITTI	0.9383	0.9041	0.9406	0.9249
KITTI + vKITTI	Proposed	vKITTI	0.9408 \pm 0.0016	0.9314 \pm 0.0013	0.9406 \pm 0.0006	0.9377 \pm 0.0011

Table 16. $\delta(1.25^2)$ of stereo-based depth estimation.